



ELSEVIER

Journal of Crystal Growth 187 (1998) 543–558

---

---

JOURNAL OF **CRYSTAL  
GROWTH**

---

---

# Convection and segregation during vertical Bridgman growth with centrifugation

W.R. Wilcox\*, L.L. Regel, W.A. Arnold<sup>1</sup>

*International Center for Gravity Materials Science and Applications, Clarkson University, Potsdam, NY 13699-5814, USA*

Received 7 August 1997; accepted 4 December 1997

---

## Abstract

Both experiments and numerical simulations have shown that centrifugation can have a large influence on convection and segregation during vertical Bridgman growth. The buoyancy-driven flow pattern differs dramatically from that observed without centrifugation. The Coriolis force introduces an azimuthal circulation that cannot be seen via the usual side view of the ampoule. The flow pattern and intensity depend on the rotation rate, centrifuge arm length, and interface shape. Several experiments and numerical simulations exhibited a minimum in axial convection or segregation at a particular rotation rate. A correlation for these results indicate that the minimum in convection occurs at a rotation rate that is independent of the centrifuge arm length, proportional to the square root of the depth of the concave interface, and inversely proportional to the ampoule radius. In attempts to better understand this minimum, three simple models have been proposed, here called “buoyancy-Coriolis balance”, “flow transition”, and “thermal stability”. The thermal stability model is developed here. Unfortunately, none of these models agree with the correlation to the published experimental and numerical results. Numerical simulations show that rotation of a vertical ampoule about its own axis at a constant rate may be a better method to control convection. © 1998 Elsevier Science B.V. All rights reserved.

---

## 1. Introduction

Convection in the melt has a strong influence on impurity segregation and crystallographic perfection resulting from directional solidification. A variety of methods have been used to influence this convection, such as vibration, microgravity, imposition of a magnetic field on electrically conducting melts, and rotation at a varying rate (ACRT). Centrifugation offers an additional method of controlling convection during crystal growth. Here, we consider primarily the vertical gradient freeze technique, in which the furnace temperature increases with height. Solidification upward is brought about by slowly decreasing the furnace temperature. The freezing interface in the gradient freeze technique is normally concave (e.g., Ref. [1]).

---

\* Corresponding author. Fax: +1 315 268 3833; e-mail: wilcox@agent.clarkson.edu.

<sup>1</sup> Present address: Goodyear Tire and Rubber Company, Akron, OH 44305-3399, USA.

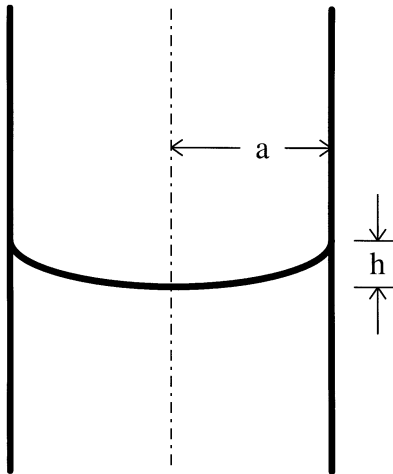


Fig. 1. Definition of interface height  $h$  (depth of concave interface).

Convection in the melt depends strongly on the interface height  $h$ , which is the difference in interface elevation between the center and the periphery (see Fig. 1).<sup>2</sup>

In 1986, Regel et al. [2] published a surprising result on silver segregation during gradient-freeze solidification of lead telluride during centrifugation.<sup>3</sup> No axial variation in doping was detected when the net acceleration  $g$  was  $5.2g_e$ , the ampoule radius was 6.5 mm, and the centrifuge radius was 18 m (Star City, Russia).<sup>4</sup> The axial variation in doping increased as  $g$  was made either larger or smaller than  $5.2g_e$ . These results indicated that convection in the melt reached a minimum at  $5.2g_e$ , where it was negligible compared to the freezing rate. Repetition of the Ag-doped PbTe experiments gave minimum axial segregation at  $2g_e$  in a centrifuge at Nantes (France) with an arm length of 5.5 m [4]. Note that although the value of  $g$  at which minimum segregation occurred for PbTe in these two centrifuges was different, the rotation rate  $\omega$  was the same. This is an important observation that we will use later in comparing the various experimental results and theoretical predictions.

Results from other centrifuge experiments have also implied either a minimum in convection at a particular  $g$ , or decreasing convection up to the maximum  $g$  investigated. Segregation in Te–Se mixtures decreased as  $g$  was increased up to  $10g_e$  in the Star City centrifuge [5]. Axial segregation in gallium-doped germanium was a minimum at a net acceleration of  $1.7g_e$  for a centrifuge arm length of 1.04 m in Erlangen (Germany), an ampoule radius of 1 cm, an initial interface height of  $\sim 0.8$  mm, and a freezing rate estimated to be  $\sim 20$  mm/h [6–8]. The thallium distribution in lead telluride became more uniform as the acceleration was increased to  $10g_e$  in the Nantes centrifuge [9]. Radial composition variations in zinc-doped cadmium

<sup>2</sup> Symbols are defined at the end in the Table of Nomenclature.

<sup>3</sup> Throughout this paper, the axis of rotation is taken as vertical. During centrifugation, the net acceleration  $g$  is aligned approximately with the ampoule axis, usually by mounting the furnace in a swing bucket attached to the end of the centrifuge arm by a hinge. If earth's gravity is defined as  $g_e$ , then  $g$  is the vector sum of  $g_e$  and the rotational acceleration,  $\omega^2 r$ , where  $\omega$  is the angular rotation rate and  $r$  is the distance from the axis of rotation.

<sup>4</sup> In Ref. [2], it was implicitly assumed that the temperature gradient inside the PbTe was equal to that set in the furnace. However, heat transfer calculations in Ref. [3] indicated that the temperature gradient inside the PbTe was about  $\frac{1}{3}$  of that assumed in Ref. [2], so that the freezing rate was about  $3 \times$  higher than reported, or  $\sim 15$  mm/h.

telluride indicated a minimum in convection at  $\sim 2g_e$  for a freezing rate of  $\sim 8$  mm/h and an ampoule radius of 5.5 mm in the 1.5 m radius Clarkson centrifuge [10]. The lamellar spacing in aluminum–copper eutectic decreased as  $g$  was increased to  $5g_e$  in the Star City centrifuge [11]. The primary dendrite spacing of tin dendrites decreased steadily up to  $15.5g_e$  in a centrifuge with 1.2 m arm at Vanderbilt University [12]. (The spacing of dendrites and eutectic lamellae decreases as convection is decreased or the freezing rate is increased.)

In efforts to understand the above experimental results, a variety of theoretical and experimental studies have been performed. These are reviewed and compared below. We begin with our current understanding of flow patterns in a gradient freeze melt during centrifugation.

## 2. Flow patterns in a gradient freeze melt during centrifugation

Fig. 2 shows schematically the basic buoyancy-driven convection that occurs without centrifugation in the vertical Bridgman configuration with a concave interface. Such flows can easily be seen in a side view by following the motion of neutrally-buoyant particles dispersed in the melt (e.g., Refs. [13,14]). The flow field in a simulated gradient freeze apparatus is being determined at Clarkson University [15,16]. Water containing neutrally-buoyant particles is placed in a cylinder that is cooled from the bottom, which is curved so as to induce a small radial temperature gradient. The slow motion of the suspended particles is recorded using a video camera and analyzed using a computer image processing system. The apparatus and the video

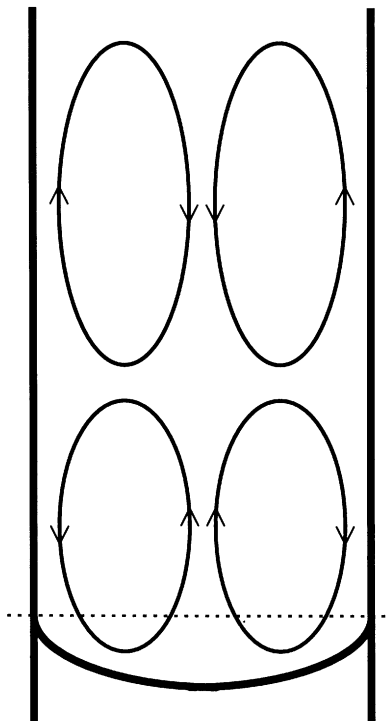


Fig. 2. Basic buoyancy-driven axisymmetric convection in the melt without centrifugation. At low rotation rates the basic pattern persists, but is masked by the circulation introduced by the Coriolis effect. The horizontal dashed line shows the viewing plane for Fig. 3.

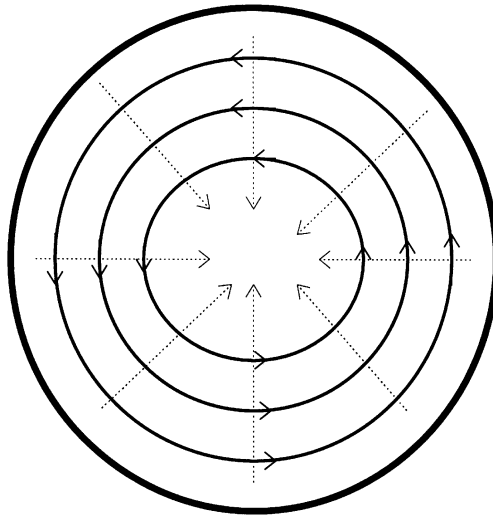


Fig. 3. Azimuthal flow due to imposition of Coriolis force on the basic flow shown in Fig. 2. Dotted arrows indicate the basic flow.

camera are placed on a swing bucket attached to the end of the centrifuge arm, so that the resultant acceleration is always directed along the axis of the experiment cylinder. Without centrifugation, an axisymmetric flow cell is set up as in Fig. 2. With centrifugation, the Coriolis force<sup>5</sup> induces an azimuthal (rotational) component to the flow that can be seen only from the bottom of the cylinder, as shown schematically in Fig. 3. This azimuthal component almost completely masks the basic buoyancy-driven convection pattern, although this pattern can be estimated by taking vectors at right angles to the observed particle motion. The observed flow pattern and velocity change slowly as the acceleration due to centrifugation is increased. One such flow pattern, often called the “shallow cavity mode”, is shown schematically in Figs. 4 and 5. The basic driving flow due to buoyancy is shown in Fig. 4. It is no longer axisymmetric because the  $g$  vector is misaligned from the ampoule axis except at one point. The Coriolis force causes the pattern near the bottom to appear as in Fig. 5. Experimentally, the side view does not appear as in Fig. 4 because the Coriolis force has distorted the flow completely. Thus, for example, a vertical illuminated sheet in the orientation shown by the dashed line in Fig. 5 shows all of the suspended particles moving nearly horizontally in one direction. The basic flow must be induced from the observed flow by taking normals to the streamlines.

<sup>5</sup> The Coriolis acceleration equals  $2\omega \times V$ , where  $\omega$  is the vector of angular rotation,  $V$  is the velocity vector, and  $\times$  denotes the vector crossproduct. Thus, the Coriolis force deflects the basic flow at right angles. It is responsible for the fact that wind in the earth's atmosphere blows along lines of constant pressure (isobars), rather than from high pressure to low pressure, relative to the earth's surface. In a region of high pressure, the air moves downward toward the earth and the Coriolis force introduces rotation relative to the earth's surface. In a low-pressure region, the air moves upward and the rotation is reversed. The situation is similar in a solidifying melt. Thus, impurity segregation, which is influenced primarily by flow normal to the freezing interface, might be expected to depend almost entirely on the basic flow and little on the Coriolis-induced rotation.

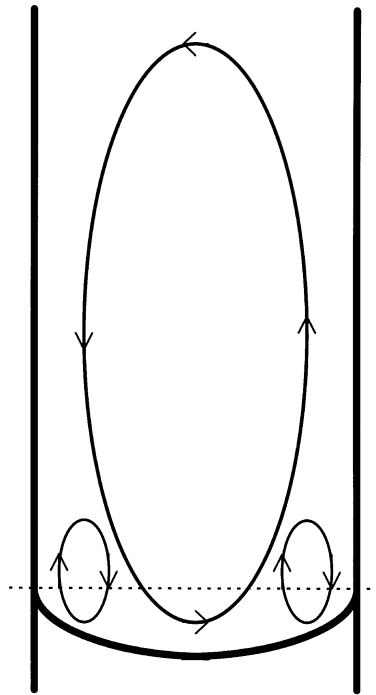


Fig. 4. Example of nonaxisymmetric basic flow caused by centrifugation. This flow is inferred by taking vectors at right angles to the azimuthal flow caused by the Coriolis effect. The dashed line shows the plane for the bottom view of this azimuthal flow shown in Fig. 5.

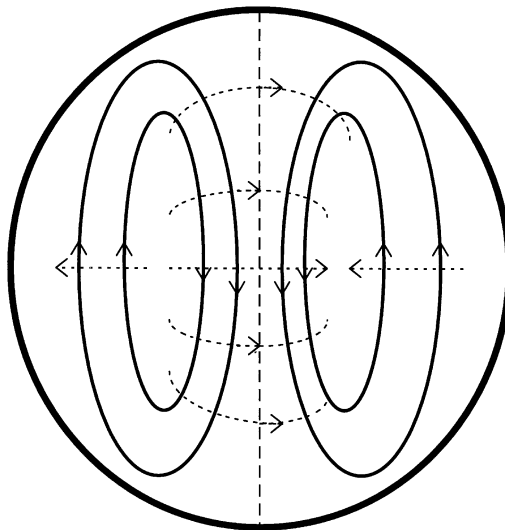


Fig. 5. Bottom view of azimuthal flow caused by action of Coriolis acceleration on basic flow shown in Fig. 4. The dotted arrows represent the basic flow if it could be seen directly (it must be inferred by taking normals to the observed streamlines.) If a side view is taken of a plane represented by the dashed line shown here, the flow will appear horizontal in one direction.

### 3. Numerical simulations

We have studied the shifts in flow modes by numerical simulations [3,17]. In the scaling analysis accompanying the nondimensionalization of the equations of motion, we developed a new dimensionless group that simplifies to

$$\text{Ad} = \frac{nL^2}{\sqrt{1 + n^2HR_c}}, \quad (1)$$

when the axial temperature gradient in the ampoule is constant. Here,  $n = \omega^2 r_c / g_e$  is the centripetal acceleration relative to earth's gravity,  $L = \ell/a$  is the aspect ratio of the melt,  $\ell$  is the length (height) of the melt,  $a$  is the ampoule radius,  $H = h/a$  is the dimensionless height of the interface,  $R_c = r_c/a$  is the dimensionless distance of the freezing interface from the axis of rotation of the centrifuge (see Fig. 6). This group represents the ratio of the buoyancy driving force for the spatially varying component of acceleration to that for the average acceleration in the melt. We suggested that for small Ad the basic convection pattern should be the usual axisymmetric mode shown in Figs. 2 and 3. At large Ad, we predicted that the convection would become nonaxisymmetric, such as that shown in Figs. 4 and 5. In a series of three-dimensional numerical simulations at  $n = 1$ , the change in flow mode took place gradually over a range of Ad from approximately 0.4 to 5.

Some numerical simulations showed a minimum in convection versus rotation rate [3,6,7,18]. For PbTe with an interface height of 0.2 mm, an ampoule radius of 6.5 mm, and a total acceleration of  $g = 1.41g_e$ , a minimum in convection was calculated at a rotation rate of 8 rad/s and a centrifuge radius of about 15 cm (see Fig. 7) [3]. For Ge with an interface height of 0.1 mm, an ampoule radius of 1 cm, and a centrifuge radius of about 1.1 m, a minimum in convection was calculated at  $\sim 1.1g_e$  [6,7,18].

### 4. Models for minimum convection conditions

Although the numerical simulations mentioned above demonstrated that a minimum in convection can be observed at a particular rotation rate, these do not readily lead to an understanding of the reason for this minimum or a convenient prediction of the rotation rate required to achieve it. Three simple models have been proposed to meet this need. We call these the flow transition model, the buoyancy-Coriolis balance model, and the thermal stability model.

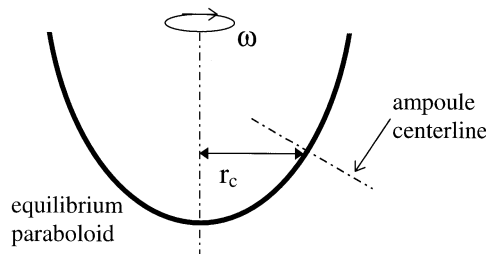


Fig. 6. Definition of  $r_c$ , which is the distance from the center of the freezing interface to the center of rotation of the centrifuge. The dark curve represents an equilibrium paraboloid. In the present analysis, the ampoule axis is normal to this paraboloid at the center of the freezing interface.

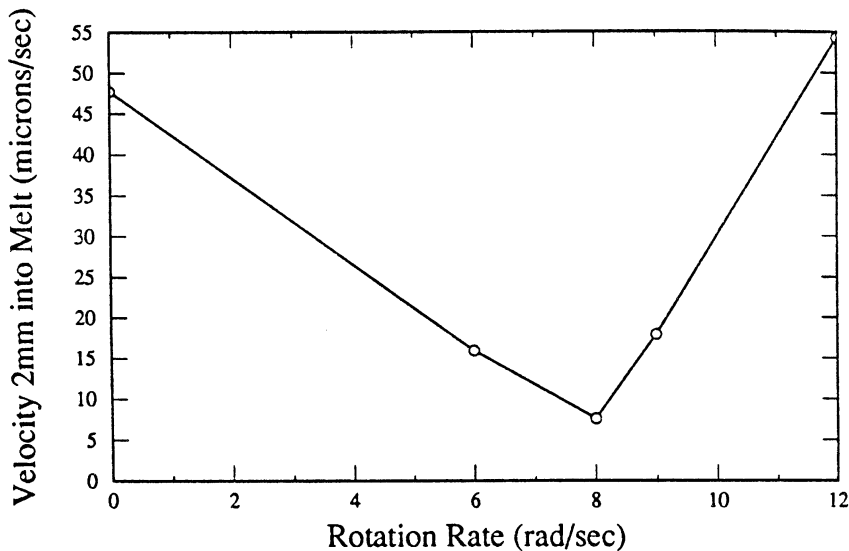


Fig. 7. Calculated melt velocity for pure PbTe along the ampoule axis 2 mm above the freezing interface, which has a constant curvature of 10.57 cm ( $h = 0.2$  mm) [2]. The net acceleration is held constant at  $g = 1.41g_e$  (for which  $n = 1$ ) by decreasing the centrifuge arm length as the rotation rate is increased according to  $r_c = 1 \times g_e/\omega^2$ . At the minimum convective velocity,  $\omega = 8 \text{ s}^{-1}$  and  $r_c = 15.3$  cm.

#### 4.1. Flow transition model

We have suggested that a minimum in convection might occur in the neighborhood of the transition from the low-acceleration flow mode to a high-acceleration flow mode, i.e. for  $Ad \approx 1$  [17]. Rearranging Eq. (1), we obtain the form required later for comparison with experimental and numerical simulation results

$$HR_c = \frac{L^2}{Ad} \frac{n}{\sqrt{1+n^2}} \quad (2)$$

#### 4.2. Buoyancy-Coriolis balance model

A simple scaling analysis suggested that the buoyancy force in the melt is balanced by the Coriolis force and that a minimum in convection should occur at  $g = 2g_e$  ( $n = \sqrt{3}$ ), independent of interface shape, centrifuge radius and material properties [19]. A more complex scaling analysis also equated the buoyancy force to the Coriolis force to predict a gentle minimum in convection at  $\sim 1.35g_e$ , with this value of  $g$  being independent of interface shape and centrifuge radius, but weakly dependent on materials properties [6,7,18]. The magnitude of the velocity at this minimum was predicted to be proportional to the rotation rate and centrifuge radius. The minimum velocity was also predicted to be proportional to the absolute value of the interface curvature, with the same retardation for both concave and convex interfaces (i.e., positive and negative values of  $H$ ).

#### 4.3. Thermal stability model

The thermal stability model stems from the observation that there would be no buoyancy-driven convection in a fluid if the net acceleration vector  $g$  were everywhere exactly parallel to the density gradient,

with density decreasing with height [3,19,20]. In a single-component system, the no-convection condition corresponds to  $g$  being normal to all isotherms in the melt. In a rotating system whose axis of rotation is vertical, the normal to  $g$  describes a paraboloidal surface. At low freezing rates, the solid-melt interface lies on an isothermal surface, at the equilibrium melting point. Thus, we would expect a minimum in convection near the freezing interface when the interface approximates a portion of a zero convection paraboloid, even though the thermal stability condition is not met throughout the entire melt. In the following, we determine the ideal interface shape that should give minimum convection because it is everywhere normal to the net acceleration  $g$ , and the dependence of this shape on acceleration and centrifuge arm length. First, we derive the equation for paraboloids normal to the net acceleration  $g$ , i.e. the equilibrium surfaces of zero convection. Second, we determine the required angle and position of the ampoule so that  $g$  at the center of the solid-liquid interface is normal to the interface and aligned with the ampoule axis. The intersection of the ampoule cylinder with the paraboloid represents the ideal interface shape required for minimum convection. Finally, the height  $h$  of the interface relative to the center is determined versus angular position  $\theta$ , acceleration  $g$  and the distance  $r_c$  of the interface center to the centrifuge's vertical axis of rotation.

Consider a liquid being rotated about a vertical axis within earth's gravity  $g_e$ .<sup>6</sup> The net acceleration vector  $g$  consists of a vertical component  $g_e$  and a radial component  $\omega^2 r$ , where  $r$  is the distance from the axis of rotation. The surface normal to this vector has the slope

$$\frac{dz}{dr} = \frac{\omega^2 r}{g_e}, \quad (3)$$

where  $z$  is height and  $r$  is the distance from the axis of rotation. Integrating Eq. (3), we obtain the equation for equilibrium paraboloids

$$z = \frac{\omega^2 r^2}{2g_e} + c, \quad (4)$$

where  $c$  is a constant that can have any value. That is, all such paraboloids at any height are valid. For example, the top surface of a rotating, nonconvecting liquid is given by this equation. For convenience in the present calculations, we take  $c = 0$ , so that the bottom center of the paraboloid is at the origin of the coordinate system.

We assume that the ampoule is cylindrical, with radius  $a$  and the center of the freezing interface at distance  $r_c$  from the centrifuge's axis. We also assume that the ampoule is oriented so that its axis is normal to the paraboloid of minimum convection at the interface position, i.e. with slope

$$\frac{dz}{dr} = -\frac{g_e}{\omega^2 r_c}. \quad (5)$$

From the viewpoint of an external spectator, the ampoule swings upward as  $\omega$  is increased. The ampoule's axis remains normal to the surface of the equilibrium paraboloid. Our concern here is with convection in the melt inside the ampoule. So we take a coordinate system fixed with respect to the ampoule and move the paraboloid until the condition given by Eq. (5) is satisfied. The intersection of the two surfaces, one cylindrical and one paraboloidal, gives the predicted interface shape for minimal convection.

Here, we use primes to denote the coordinate system for the cylindrical ampoule. We nondimensionalize by dividing distances by the ampoule radius  $a$  and accelerations by earth's gravity  $g_e$ . Dimensionless distances are denoted by capital letters. We see that the ideal interface shape in dimensionless form must be

<sup>6</sup> The container for this liquid need not be centered on the axis of rotation, although it may be.

a function of  $n = \omega^2 r_c / g_e$  and  $R_c = r_c / a$ , i.e. the relative centrifugal acceleration and the dimensionless distance of the freezing interface to the centrifuge axis.

The equation for the cylindrical ampoule in its dimensionless coordinate system is

$$1 = R^2 = X^2 + Y^2. \tag{6}$$

The center of the freezing interface is taken to be at the origin of this coordinate system with zero slope. We consider that the paraboloid of minimum convection is rotated upward by angle  $\varphi = \arctan(n)$  in the  $X$ – $Z$  plane ( $Y$  held constant). For the paraboloid to intersect the center of the freezing interface, it must also be translated in both  $x'$  and  $y'$  directions, so that the relationship between the coordinate systems is

$$\begin{aligned} x &= (x' + f) \cos(\varphi) - (z' - e) \sin(\varphi), \\ z &= (x' + f) \sin(\varphi) + (z' - e) \cos(\varphi), \\ y &= y'. \end{aligned} \tag{7}$$

Substituting these into Eq. (4) with  $c = 0$  and nondimensionalizing, we obtain for the paraboloid

$$0 = -Y^2 + 2 \frac{R_c [n(X + F) + Z - E]}{n\sqrt{1 + n^2}} - \frac{[X + F - n(Z - E)]^2}{1 + n^2}. \tag{8}$$

The values of  $E$  and  $F$  are found<sup>7</sup> by requiring that the paraboloid intersect the origin (the center of the freezing interface) and that the slope ( $\partial Z / \partial X$ ) be zero at the origin

$$E = \frac{nR_c}{2\sqrt{1 + n^2}}, \tag{9}$$

$$F = \frac{(2 + n^2)R_c}{2\sqrt{1 + n^2}}. \tag{10}$$

Fig. 8 shows a paraboloid and ampoule for an ampoule radius that is 1/10 of the distance of the center of the interface from the axis of rotation, i.e.  $R_c = 10$ . The centrifugal acceleration is equal to earth's gravity ( $n = 1$ ), so that the ampoule's axis is actually 45° from vertical. Note that this section of the zero-convection paraboloid is *not* axisymmetric with respect to the ampoule.

To find the ideal interface shape, we solve for  $Z$ , which is the interface height within the cylinder ( $X^2 + Y^2 \leq 1$ )

$$Z = \frac{(1 + n^2)^{3/2} R_c + n^2 X - \sqrt{1 + n^2} \sqrt{(1 + n^2)^2 R_c^2 - n^4 Y^2 + 2n^2 \sqrt{1 + n^2} R_c X}}{n^3}. \tag{11}$$

For  $R_c = 10$  and  $n = 1$ , Fig. 9 shows the contours of the ideal interface looking down from above within the ampoule. Fig. 10 shows an example of an ideal interface for  $R_c = 10$  and  $n = 100$ . For these conditions, the shape is completely nonaxisymmetric. This section of the paraboloid is virtually cylindrical at a right angle to the ampoule, which is nearly horizontal. The constant elevation contours are, effectively, parallel straight lines. This nonaxisymmetry is apparent when we examine the height  $H$  of the interface at the ampoule surface ( $X^2 + Y^2 = 1$ ), as shown in Fig. 11. For  $n \gg 1$ , the dependence of  $H$  on angular position is essentially sinusoidal.

---

<sup>7</sup>The mathematical manipulations were performed and the plots prepared using the computer algebra system, Maple V Release 4, from Waterloo Maple Inc., Waterloo, Ontario, Canada N2L 5J2.

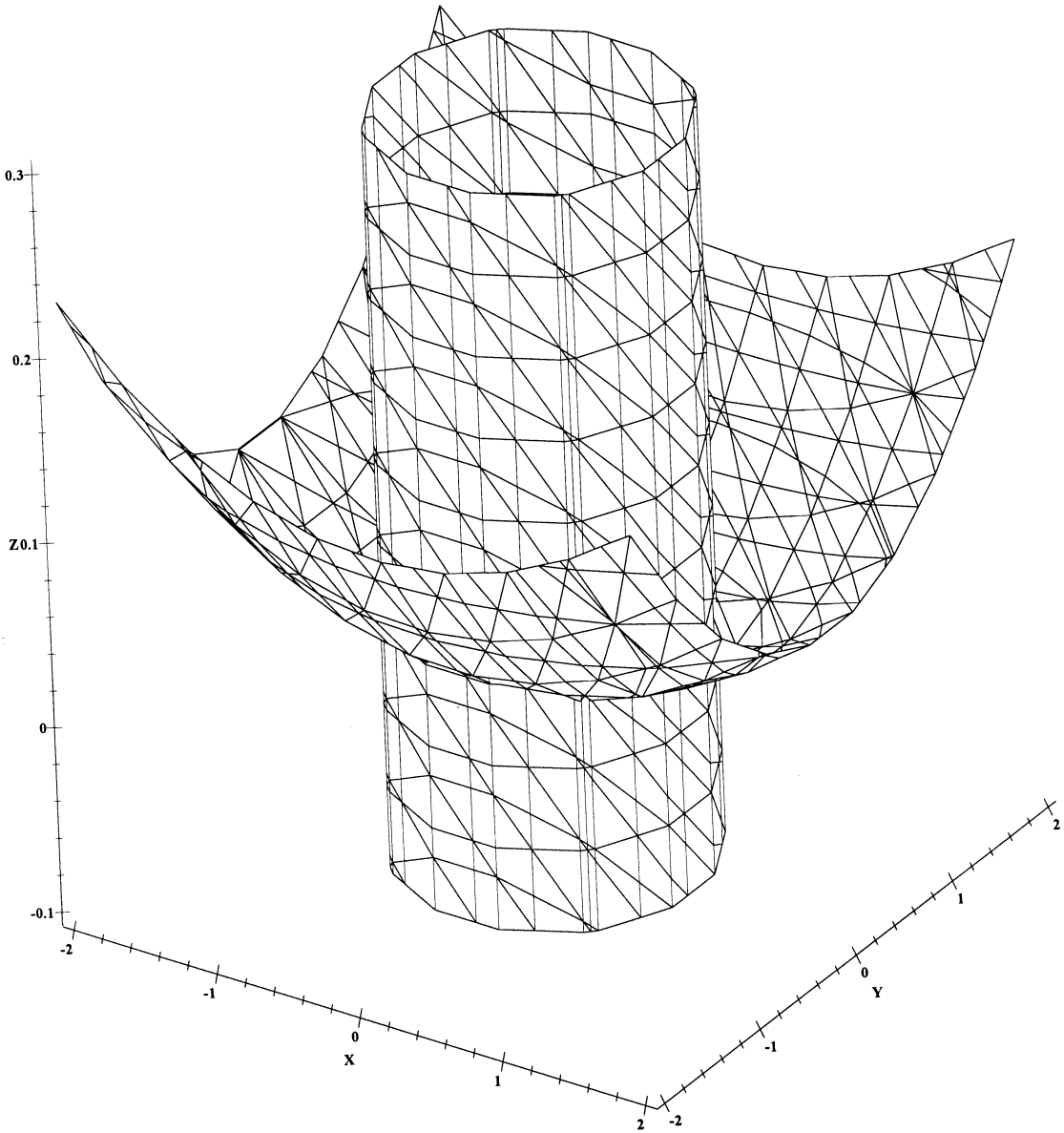


Fig. 8. A cylindrical ampoule intersecting an equilibrium paraboloid for  $R_c = 10$  and  $n = 1$ . Rotate this figure by  $45^\circ$  to see the actual ampoule position for this value of  $n$ .

The maximum value of the interface height is found by substituting  $Y^2 = X^2 + 1$  in Eq. (11) and differentiating with respect to  $X$

$$H_{\max} = \frac{R_c \sqrt{1 + n^2} - \sqrt{R_c^2(1 + n^2) - n^2}}{n}. \quad (12)$$

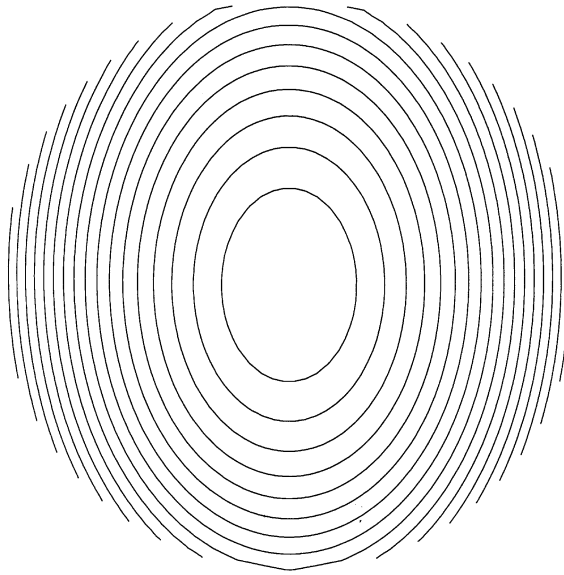


Fig. 9. View downward along the ampoule axis of the intersection of a cylindrical ampoule with an equilibrium paraboloid for  $R_c = 10$  and  $n = 1$ . The contour lines are at equal increments of elevation, with the center being the lowest elevation.

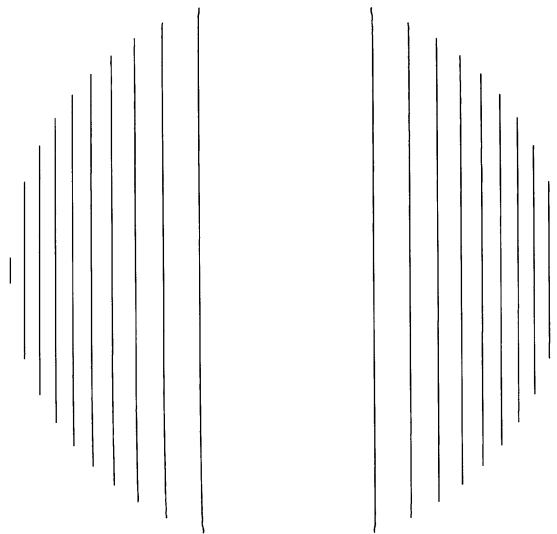


Fig. 10. Contours for the equilibrium surface for  $R_c = 10$  and  $n = 100$ .

For the large centrifuges used in materials processing research, Eq. (12) becomes

$$H_{\max}R_c = \frac{n}{2\sqrt{1+n^2}} \quad \text{for } R_c \gg 1. \tag{13}$$

Note that this has the same functional dependence as Eq. (2) for the predicted transition of flow patterns, but differs by a constant  $Ad/2L^2$ . The asymptotic value of Eq. (13) for  $n \ll 1$  is  $HR_c = n/2$ , which can be derived

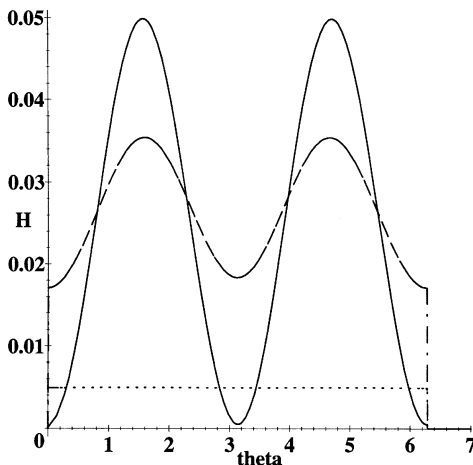


Fig. 11. Height  $H$  of the interface at the ampoule wall versus angle  $\theta$  for  $R_c = 10$  and: (-----)  $n = 0.1$ ; (-·-·-)  $n = 1$ ; (—)  $n = 10$ .

from Eq. (4) for an ampoule rotated about its own axis ( $z = h$  at  $r = a$ ). If we substitute the definitions of  $H$ ,  $R_c$  and  $n$  into this low rotation rate form, we find that  $r_c$  cancels out and

$$\omega = \frac{\sqrt{2hg_e}}{a} \quad \text{for } \omega \ll \sqrt{\frac{2g_e}{r_c}}. \quad (14)$$

That is, under these conditions of large centrifuge arm length and low rotation rate, the thermal stability model predicts a minimum in convection at a rotation rate that is independent of the arm length of the centrifuge.

The minimum interface height  $H_{\min}$  occurs at  $\theta = 0$ , which corresponds to  $Y = 0$  and  $X = 1$  in Eq. (11). For small accelerations we find  $HR_c = n/2$ , which is the same result as Eq. (14). This is not surprising as the interface is axisymmetric for small rotation rates when the ampoule is nearly vertical. This is valid for  $n \leq 1$  with  $R_c \rightarrow \infty$ . For large accelerations on the other hand

$$H_{\min}R_c = \frac{1}{2n^2} \quad \text{for } n \gg 1 \quad (15)$$

which is valid for  $n \geq 1$  with  $R_c \rightarrow \infty$ .

#### 4.4. Comparison of predictions and experiments for minimum convection or segregation

Table 1 summarizes the experimental results and theoretical predictions for minimum convection conditions.

These data and predictions are plotted in Fig. 12. Also, shown in Fig. 12 is a least-squares fit to the experimental and numerical data points, imposing the condition that it be linear with zero intercept to fit the observation that minimum convection in Regel et al.'s PbTe experiments on two different centrifuges occurred at the same rotation rate [2,4]. The equation for this line is

$$HR_c = 2.8n, \text{ or } \omega = \sqrt{\frac{hg_e}{2.8a^2}}. \quad (16)$$

Table 1  
Summary of experimental results and theoretical predictions for minimum convection conditions

Source	Code in Fig. 12	$n = \omega^2 r_c / g_c$	$HR_c = hr_c / a^2$	Notes	Refs.
PbTe Star City experiments	E-1	5.1	~ 14	H assumed 0.005	[2,4]
PbTe Nantes experiments	E-2	~ 1.7	~ 4	H assumed 0.005	[4]
Ge Erlangen experiments	E-3	1.4	~ 8	H from initial interface	[6–8]
PbTe numerical calculations	T-1	1.00	0.71		[3]
Ge numerical calculations	T-2	0.46	1.1		[6,7,18]
Buoyancy–Coriolis model	C-1	1.73	all		[19]
Buoyancy–Coriolis model	C-2	0.91	all		[6,7,18]
Thermal stability model	—		$n/2 (1 + n^2)^{1/2}$	Eq. (13)	[3]
Flow transition model	---		$16 n / (1 + n^2)^{1/2}$	Eq. (2) with $Ad = 1, L = 4$	[3]

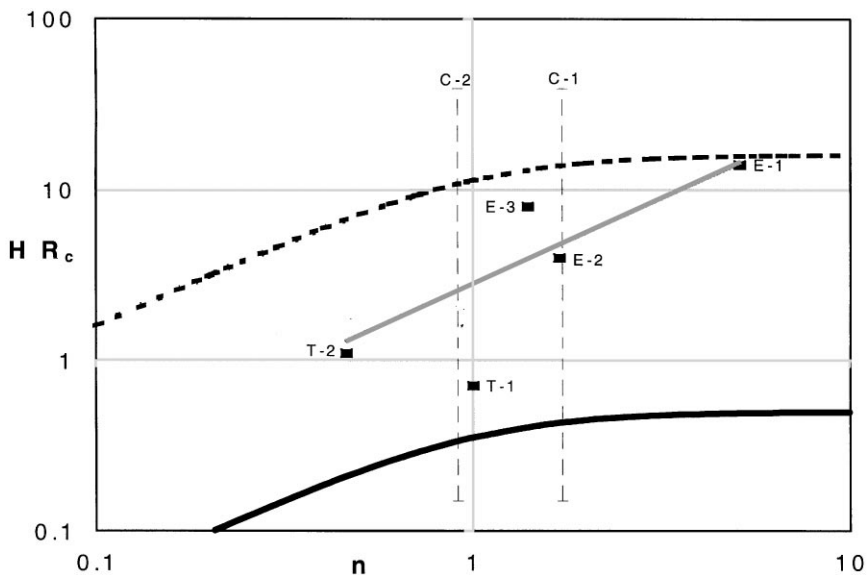


Fig. 12. Experimental results and theoretical predictions for minimum convection and segregation conditions. Table 1 contains the codes for the symbols in this figure. Here the *E* denotes an experimental value and *T* a numerical simulation result. The dashed curve represents the flow transition model (Eq. (2) with  $L = 4$  and  $Ad = 1$ ). The lower solid curve is the thermal stability model prediction (Eq. (13)). The vertical lines labeled *C* are the buoyancy-Coriolis balance model predictions. The middle solid line is the equation (Eq. (16)) that best correlates the experimental and numerical simulation values.

We note that this result does not agree with any of the three simple models, particularly the Buoyancy–Coriolis model that predicts minimum convection at a particular  $n$  independent of  $H$  and  $R_c$ . It does lie between the thermal stability and flow transition models and has the same slope as these models for  $n \ll 1$ . Thus, it appears that in centrifugation the dependence of convective vigor on the experimental parameters is more complex than predicted by any of the three simple models that have been proposed.

## 5. Rotation of a vertical ampoule about its own axis

The correlating Eq. (16) predicts that the rotation rate for minimum convection is independent of the arm length of the centrifuge. In the limit, we can consider an arm length of zero, i.e. a vertical ampoule rotated about its own axis. This is simpler to analyze because of the axisymmetric variation of acceleration throughout the fluid. We have carried out numerical simulations of buoyancy-driven convection in a vertical ampoule being rotated about its own axis [3,20,21]. Without rotation, the flow is axisymmetric, as shown in Fig. 2. With rotation at low rates, the same basic flow pattern continues, but superimposed on it is a strong rotational component due to the Coriolis effect (Fig. 3). As the rotation rate is increased, a minimum occurs in convective velocity versus rotation rate. For a paraboloidal interface shape, this minimum is sharp and occurs exactly at the rotation rate predicted from the thermal stability model (Eq. (14)) [20]. With a spherical concave interface, the minimum in convective velocity is much less sharp, but remains near that predicted by Eq. (14) [21]. At rotation rates larger than that yielding a minimum in convection, the flow directions are the reverse of those shown in Figs. 2 and 3.

## 6. Conclusions

A variety of numerical simulations and experimental results have demonstrated that centrifugation can reduce buoyancy-driven convection and segregation in vertical Bridgman techniques. Under some conditions, a minimum is produced at a particular rotation rate. A correlation of these results suggests that this rotation rate is independent of the arm length of the centrifuge. None of the three simple models that have been proposed to explain this minimum agree with this correlation, although it lies between the low rotation rate predictions for the thermal stability model and the flow transition model.

Numerical simulations suggest that the simplest method to take advantage of these centrifugal effects is to rotate a vertical ampoule about its own axis. With a concave interface, a minimum in convection can be produced at a rotation rate predicted by the thermal stability model. Beyond this rotation rate the flow reverses in direction, which may be useful for certain applications such as detached solidification [22].

## Nomenclature

$a$	ampoule radius (m)
$Ad$	Arnold number $-\omega_2 \Delta T_a \ell / g \Delta T_r$ – for constant axial temperature gradient, $= nL^2 / (n+1)HR_c$ (dimensionless)
$c$	constant of integration in Eq. (2) (m) (here, $c = 0$ )
$e$	distance by which paraboloid is translated in $z'$ direction after rotation into coordinate system of ampoule (m)
$E$	$e/a$ – dimensionless translation distance in $Z$ direction
$f$	distance by which paraboloid is translated in $-x'$ direction after rotation into coordinate system of ampoule (m)
$F$	$f/a$ – dimensionless translation distance in $-X$ direction
$g$	net acceleration; vector sum of $g_e + \omega^2 r$ , with value of $\sqrt{g_e + \omega^2 r}$
$g_e$	acceleration due to earth's gravity ( $9.8 \text{ m/s}^2$ ). Directed in negative $z$ direction.
$h$	interface height at the ampoule wall relative to the elevation at the center (m) (a function of angular position $\theta$ , except when the ampoule is rotated about its own axis)
$H$	$h/a$ – dimensionless interface height
$H_{\max}$	the maximum value of $H$ , which occurs at $\theta = 0$ ( $Y = 0, X = 1$ )

$H_{\min}$	the minimum value of $H$ . For $R_c \gg 1$ , this occurs at $\theta = \pi/2$ and $3\pi/2$
$\ell$	length (height) of the melt above the freezing interface (m)
$L$	$\ell/a$ – aspect ratio for the melt column, i.e. its dimensionless height
$n$	relative value of centripetal acceleration at center of freezing interface, $\omega^2 r_c / g_c = \sqrt{(g/g_c) - 1}$
$r$	distance from the centerline of rotation (m)
$r'$	distance from the ampoule axis (m)
$R$	$r'/a = X^2 + Y^2$ – dimensionless radial position
$r_c$	distance of the center of the freezing interface from the centrifuge axis (m)
$R_c$	$r_c/a$ – dimensionless radius of centrifuge
$\Delta T_a$	axial difference in temperature between the bottom and the top of the melt in the ampoule (K)
$\Delta T_r$	radial difference in temperature between the center and the ampoule wall (K)
$x'$	distance to the right of the ampoule axis (m)
$X$	$x'/a$ – dimensionless distance in ampoule coordinate system
$y'$	distance to the back of the ampoule axis (m)
$Y$	$y'/a$ – dimensionless distance in ampoule coordinate system
$z$	vertical distance upward along axis of rotation (m)
$z'$	vertical distance upward along the ampoule axis from the center of the freezing interface (m)
$Z$	$z'/a$ – dimensionless distance upward in ampoule coordinate system

### Greek letters

$\omega$	angular rotation rate about $z$ axis (rad/s)
$\varphi$	angle by which the ampoule must be rotated for $g$ to be parallel to the ampoule's axis at the center of the interface, $\tan^{-1}(n)$
$\theta$	angular position about ampoule axis from $x'$ axis

### Acknowledgements

This research was supported by NSF grant DMR-9414304.

### References

- [1] V. Yip, C. Chang, W.R. Wilcox, *J. Crystal Growth* 22 (1974) 247.
- [2] H. Rodot, L.L. Regel, G.V. Sarafanov, H. Hamidi, I.V. Videskii, A.M. Turtchaninov, *J. Crystal Growth* 79 (1986) 77.
- [3] W.A. Arnold, PhD Thesis, Clarkson University, Potsdam, New York, 1994.
- [4] H. Rodot, L.L. Regel, A.M. Turtchaninov, *J. Crystal Growth* 104 (1990) 280.
- [5] L.L. Regel, A.M. Turtchaninov, Preprint Pr-1474, Institut Kosmicheskii Issledovaniye, Akademii Nauk SSSR, Moscow, 1989.
- [6] J. Friedrich, J. Baumgartl, H.-J. Leister, G. Müller, *J. Crystal Growth* 167 (1996) 45.
- [7] J. Friedrich, PhD Thesis, Universität Erlangen-Nürnberg, Erlangen, Germany, 1996.
- [8] J. Friedrich, G. Müller, in: L.L. Regel, W.R. Wilcox (Eds.), *Centrifugal Materials Processing*, Plenum Press, New York, 1997, pp. 29–43.
- [9] R. Parfeniev, D. Shamshur, L.L. Regel, S. Nemov, in: L.L. Regel, W.R. Wilcox (Eds.), *Centrifugal Materials Processing*, Plenum Press, New York, 1997, pp. 109–114.
- [10] L.O. Ladeira, J. Shen, L.L. Regel, W.R. Wilcox, in: L.L. Regel, W.R. Wilcox (Eds.), *Centrifugal Materials Processing*, Plenum Press, New York, 1997, pp. 133–146.
- [11] L.L. Regel, I.V. Videskii, V.V. Zubenko, I.M. Safonova, I.V. Telegina, *Fiz. Khim. Obr. Mater.* 23 (1988) 45.

- [12] R.N. Grugel, A.B. Hmelo, C.C. Battaile, T.G. Wang, in: L.L. Regel, W.R. Wilcox (Eds.), *Materials Processing in High Gravity*, Plenum Press, New York, 1994, pp. 101–110.
- [13] G.T. Neugebauer, W.R. Wilcox, *J. Crystal Growth* 89 (1988) 143–154.
- [14] G.T. Neugebauer, W.R. Wilcox, *Acta Astronautica* 25 (1991) 357.
- [15] P.V. Skudarnov, L.L. Regel, W.R. Wilcox, in: L.L. Regel, W.R. Wilcox (Eds.), *Centrifugal Materials Processing*, Plenum Press, New York, 1997, pp. 75–88.
- [16] P.V. Skudarnov, Clarkson University, 1997, private communication.
- [17] W.A. Arnold, W.R. Wilcox, F. Carlson, A. Chait, L.L. Regel, *J. Crystal Growth* 119 (1992) 24.
- [18] J. Friedrich, G. Müller, in: L.L. Regel, W.R. Wilcox (Eds.), *Centrifugal Materials Processing*, Plenum Press, New York, 1997, pp. 17–28.
- [19] V.A. Urpin, in: L.L. Regel, W.R. Wilcox (Eds.), *Materials Processing in High Gravity*, Plenum Press, New York, 1994, pp. 35–41.
- [20] W.A. Arnold, L.L. Regel, in: L.L. Regel, W.R. Wilcox (Eds.), *Materials Processing in High Gravity*, Plenum Press, New York, 1994, pp. 17–34.
- [21] W.A. Arnold, L.L. Regel, in: L.L. Regel, W.R. Wilcox (Eds.), *Centrifugal Materials Processing*, Plenum Press, New York, 1997, pp. 59–74.
- [22] D.I. Popov, L.L. Regel, W.R. Wilcox, *J. Mat. Synth. Proc.* 5 (1997) 313.